Journal of Applied Mechanics and Technical Physics, Vol. 48, No. 1, pp. 135–144, 2007

STABILITY REGION OF A CLOSE-PACKED LAYER OF ATOMS

N. S. Astapov and V. M. Kornev

UDC 539.3

A rhombic four-atom unit cell corresponding to a close-packed atomic layer is considered, The interatomic forces in the cell are defined by the Morse and Lennard-Jones potentials for large strains. The stability region of the cell is constructed as a function of two parameters that model tension–compression along the major diagonal of the cell and shear. For each point in the stability region, equilibrium states of the cell are determined numerically; at least one of these states is stable. It is shown that for the close-packed atomic layer under combined compression–shear loading, Poisson's ratio needs to be taken into account.

Key words: *Close-packed atomic layer, four-atom cell, Morse and Lennard-Jones potentials, shear, tension–compression, stability region.*

Introduction. Solid-state theory, which explains, in particular, deformation and strength properties, is based on quantum mechanics. Using the quantum-mechanical approach, one can exactly calculate all empirical constants in the phenomenological theories of elasticity, plasticity, creep, fracture, etc., provided the structure and chemical composition of the body are known [1]. The existing fracture criteria, supported experimentally, correspond to complex microphysical fracture processes that occur at the structural-cell scale and lead to macrodefects. However, problem formulations that explicitly take into account the atomic structure of materials complicate the solution so that one usually has to use a deformable solid model [1] instead or consider several different models, each of which describes phenomena at the spatial scale inherent in these models: the smaller the dimension of a model that admits extrapolation to large scales, the wider the range of conditions which can be predicted or interrelated based on available experimental data [2]. Therefore, as a first step in solving quantum-mechanical problems, it is reasonable to perform static stability analysis using Newtonian mechanics. In this step, as a rule, one obtains the full information required to describe the macroscopic mechanical properties of the solid [1, 3].

One of the objectives of such studies is to predict failure at the stress-concentration sites in loaded solids using calculated critical loads [3]. For example, Macmillan and Kelly [4] studied the static stability of an ideal crystal in a Newtonian approximation using semi-empirical Lennard-Jones and Born–Mayer type potentials to describe atomic interaction. It should be noted that the parameters in the expression for the model potential are chosen so that the physical quantities due to interatomic interaction calculated using this potential are equal or reasonably close to the experimental values. In this case, the sum of the force potential and the effective interatomic energy is used as the total potential energy function of the system to study the effect of external conservative forces on the mechanical behavior of the crystal. Although the interatomic forces for almost all metals are not central even approximately, the main contribution to the energy change due to a change in the atomic configuration for a constant atomic volume can be determined as the work of central interaction forces. Therefore, even if noncentral interactions make a great contribution to the atomic-lattice energy, one can obtain adequate estimates of some properties by using a simple model of pair central interactions [1, 5–7].

Thompson and Shorrock [8] showed how the planar displacement field of a close-packed atomic layer produced by uniform strains can be used to construct an admissible displacement field for a face-centered cubic lattice with

Lavrent'ev Institute of Hydrodynamics, Siberian Division, Russian Academy of Sciences, Novosibirsk 630090; nika@hydro.nsc.ru, kornev@hydro.nsc.ru. Translated from Prikladnaya Mekhanika i Tekhnicheskaya Fizika, Vol. 48, No. 1, pp. 161–172, January–February, 2007. Original article submitted July 1, 2005; revision submitted March 20, 2006.

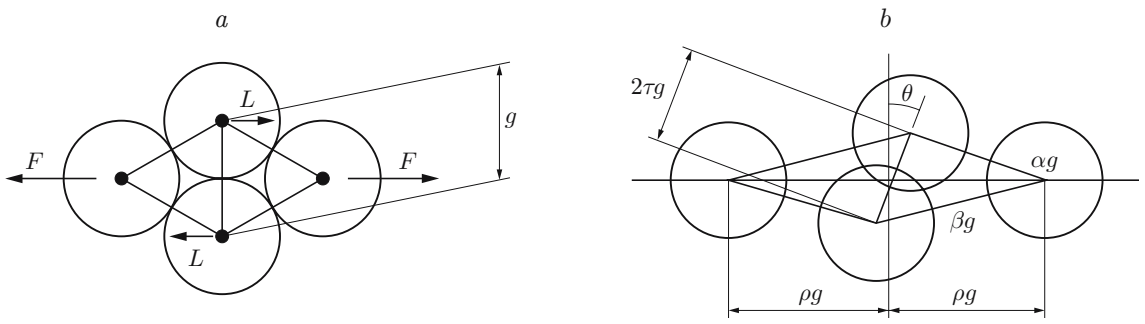

Fig. 1. Four-atom unit cell: (a) undeformed state; (b) extension along the diagonal.

uniform strains. Under certain assumptions, the total potential energy of an infinite layer is proportional to the energy of a unit cell consisting of four atoms; it is therefore important to study in detail the behavior of the unit cell since it largely determines the behavior of the entire system [3]. Using the Lennard-Jones and Morse model potentials, it has been shown [8, 9] that the occurrence of shear leads to premature instability of the unit cell.

In the present paper, the stability of a planar four-atom unit cell under large strains is studied using the approach outlined in [1, 8, 9] taking into account Poisson's effect.

Formulation of the Problem. We assume that the interaction potential energy of any two atoms is a certain function $v(\gamma)$ — the spherically symmetric potential of interaction of two solids for which the interaction force is directed along the line through their centers (γ is the dimensionless distance between the centers). We confine our attention to the interaction between the nearest-neighbor atoms and assume that the four-atom unit cell is shaped like a rhomb with the distance between the centers of the two middle atoms equal to the atomic diameter g (Fig. 1a). We recall that previous studies [1, 8, 9] dealt only with the case of extension in the normal direction to the close-packed layer, where the stress applied to the layer tends to force apart the atomic chains, may rotate them, but does not change their length. Unlike in the approaches mentioned above, we additionally take into account interaction effects between the two middle atoms in the cell using the dimensionless distance 2τ between their centers: in [1, 8, 9], it was assumed that $\tau = 1/2$, but we consider any values of $\tau > 0$. However, the calculation results show that the solutions are in the narrow interval of $0.40 < \tau < 0.65$. Thus, the condition of undeformable vertical chains is weakened, which allows us to take into account Poisson's effect and the change in the cell configuration due to compression.

Figure 1a shows the undeformed cell and Fig. 1b (taken from [3, Fig. 69]) shows a rhombic cell stretched along the diagonal. The independent generalized coordinates ρ, θ, and τ define the deformed state of the unit cell; for the ideal system (ignoring shear), $\theta = 0$. We introduce two dependent variables α and β — the dimensionless distances between the atomic pairs (Fig. 1b) such that $\alpha = \beta = 1$, $\theta = 0$, $\tau = 1/2$, and $\rho = \sqrt{3}/2$ for the unloaded state. The variables α and β are related to ρ, θ, and τ by the formulas

$$\alpha^2 = \tau^2 + \rho^2 - 2\tau\rho\sin\theta, \qquad \beta^2 = \tau^2 + \rho^2 + 2\tau\rho\sin\theta. \tag{1}$$

We consider the deformation of the system subjected to forces F and L directed along the major diagonal of the rhomb (Fig. 1a). We write the total potential energy function of the unit cell as [3]

$$V(\rho, \theta, \tau, F, L) = 2v(\alpha) + 2v(\beta) + v(2\tau) - 2F\rho g - 2L\tau g\sin\theta. \tag{2}$$

A minimum of the function V provides a sufficient condition for the stable equilibrium of the system. We study the stability of a planar four-atom unit cell using the Lennard-Jones and Morse potentials as the interaction potentials of two atoms $v(\gamma)$.

Solution Algorithm. For the given forces F and L, the equilibrium state of the cell is determined from the condition that the derivatives of the total potential energy function vanish, i.e., from the system of three nonlinear equations for three unknowns ρ, θ, and τ:

$$V_\rho = 0, \qquad V_\theta = 0, \qquad V_\tau = 0. \tag{3}$$

The stability of the equilibrium state is checked by the Hessian matrix of second-order derivatives using the Sylvester criterion. It is obvious that the unit cell is stable at the coordinate origin, i.e., at the point $F = 0$, $L = 0$. To

construct the stability region, we fix a point in the plane (F, L), say F, and study the stability of this point by varying the second coordinate $L = i\Delta L$ $(i = 0, 1, 2, \ldots)$ with a certain increment ΔL. Thus, we obtain the boundary of the stability region of the cell in the plane (F, L). The stability region is symmetric about the axis OF and with respect to a change in the sign of L; therefore, from physical considerations, only calculation results for positive values of L are given below.

Stability Region for the Morse Potential. We write the Morse potential as [5, 6]

$$v(\gamma) = Ag^{-6}\,(\mathrm{e}^{-2b(\gamma-1)}/2 - \mathrm{e}^{-b(\gamma-1)}), \tag{4}$$

where A, b, and g are parameters that depend on the type of atom. The first- and second-order partial derivatives of the functions $\alpha(\rho, \theta, \tau)$ and $\beta(\rho, \theta, \tau)$ with respect to ρ, θ, and τ are found from relations (1) as derivatives of implicit functions:

$$\begin{gathered}
\alpha_\rho = (\rho - \tau\sin\theta)/\alpha, \qquad \alpha_\theta = -\rho\tau\cos\theta/\alpha, \qquad \alpha_\tau = (\tau - \rho\sin\theta)/\alpha,\\
\beta_\rho = (\rho + \tau\sin\theta)/\beta, \qquad \beta_\theta = \rho\tau\cos\theta/\beta, \qquad \beta_\tau = (\tau + \rho\sin\theta)/\beta,\\
\alpha_{\rho\rho} = \tau^2\cos^2\theta/\alpha^3, \qquad \alpha_{\rho\theta} = \tau^2\cos\theta(\rho\sin\theta - \tau)/\alpha^3, \qquad \alpha_{\rho\tau} = -\rho\tau\cos^2\theta/\alpha^3,\\
\alpha_{\theta\theta} = \rho\tau(\alpha^2\sin\theta - \rho\tau\cos^2\theta)/\alpha^3, \qquad \alpha_{\theta\tau} = \rho^2\cos\theta(\tau\sin\theta - \rho)/\alpha^3,\\
\beta_{\rho\rho} = \tau^2\cos^2\theta/\beta^3, \qquad \beta_{\rho\theta} = \tau^2\cos\theta(\rho\sin\theta + \tau)/\beta^3, \qquad \beta_{\rho\tau} = -\rho\tau\cos^2\theta/\beta^3,\\
\beta_{\theta\theta} = -\rho\tau(\beta^2\sin\theta + \rho\tau\cos^2\theta)/\beta^3, \qquad \beta_{\theta\tau} = \rho^2\cos\theta(\tau\sin\theta + \rho)/\beta^3,\\
\alpha_{\tau\tau} = \rho^2\cos^2\theta/\alpha^3, \qquad \beta_{\tau\tau} = \rho^2\cos^2\theta/\beta^3.
\end{gathered} \tag{5}$$

Using relations (2), (4), and (5), we write system (3) as

$$(\mathrm{e}^{-2b(\alpha-1)} - \mathrm{e}^{-b(\alpha-1)})(\rho - \tau\sin\theta)/\alpha + (\mathrm{e}^{-2b(\beta-1)} - \mathrm{e}^{-b(\beta-1)})(\rho + \tau\sin\theta)/\beta + f = 0; \tag{6}$$

$$\rho(\mathrm{e}^{-2b(\beta-1)} - \mathrm{e}^{-b(\beta-1)})/\beta - \rho(\mathrm{e}^{-2b(\alpha-1)} - \mathrm{e}^{-b(\alpha-1)})/\alpha + l = 0; \tag{7}$$

$$\begin{gathered}
(\mathrm{e}^{-2b(\alpha-1)} - \mathrm{e}^{-b(\alpha-1)})(\tau - \rho\sin\theta)/\alpha + (\mathrm{e}^{-2b(2\tau-1)} - \mathrm{e}^{-b(2\tau-1)})\\
+ (\mathrm{e}^{-2b(\beta-1)} - \mathrm{e}^{-b(\beta-1)})(\tau + \rho\sin\theta)/\beta + l\sin\theta = 0,
\end{gathered} \tag{8}$$

where $f = Fg^7/(bA)$ and $l = Lg^7/(bA)$. Elimination of l from Eqs. (7) and (8), yields the equation

$$(\mathrm{e}^{-2b(\alpha-1)} - \mathrm{e}^{-b(\alpha-1)})\tau/\alpha + \mathrm{e}^{-2b(2\tau-1)} - \mathrm{e}^{-b(2\tau-1)} + (\mathrm{e}^{-2b(\beta-1)} - \mathrm{e}^{-b(\beta-1)})\tau/\beta = 0, \tag{9}$$

which, together with (6) and (7), is equivalent to system (6)–(8) or system (3) for determining the equilibrium state of the unit cell for given F and L in the case of the Morse potential. Substitution of the solutions (ρ, θ, τ) of system (6), (7), (9) into the expression for the second derivatives of function (2) yields

$$\begin{gathered}
V_{\rho\rho} = b(2\,\mathrm{e}^{-2b(\alpha-1)} - \mathrm{e}^{-b(\alpha-1)})(1 - \tau^2\cos^2\theta/\alpha^2)\\
- (\mathrm{e}^{-2b(\alpha-1)} - \mathrm{e}^{-b(\alpha-1)})\tau^2\cos^2\theta/\alpha^3 - (\mathrm{e}^{-2b(\beta-1)} - \mathrm{e}^{-b(\beta-1)})\tau^2\cos^2\theta/\beta^3\\
+ b(2\,\mathrm{e}^{-2b(\beta-1)} - \mathrm{e}^{-b(\beta-1)})(1 - \tau^2\cos^2\theta/\beta^2),\\
V_{\rho\theta} = \tau\cos\theta[-b(2\,\mathrm{e}^{-2b(\alpha-1)} - \mathrm{e}^{-b(\alpha-1)})\rho(\rho - \tau\sin\theta)/\alpha^2\\
+ (\mathrm{e}^{-2b(\alpha-1)} - \mathrm{e}^{-b(\alpha-1)})\tau(\tau - \rho\sin\theta)/\alpha^3 - (\mathrm{e}^{-2b(\beta-1)} - \mathrm{e}^{-b(\beta-1)})\tau(\tau + \rho\sin\theta)/\beta^3\\
+ b(2\,\mathrm{e}^{-2b(\beta-1)} - \mathrm{e}^{-b(\beta-1)})\rho(\rho + \tau\sin\theta)/\beta^2],\\
V_{\rho\tau} = b(2\,\mathrm{e}^{-2b(\alpha-1)} - \mathrm{e}^{-b(\alpha-1)})(\rho - \tau\sin\theta)(\tau - \rho\sin\theta)/\alpha^2\\
+ (\mathrm{e}^{-2b(\alpha-1)} - \mathrm{e}^{-b(\alpha-1)})\rho\tau\cos^2\theta/\alpha^3 + (\mathrm{e}^{-2b(\beta-1)} - \mathrm{e}^{-b(\beta-1)})\rho\tau\cos^2\theta/\beta^3\\
+ b(2\,\mathrm{e}^{-2b(\beta-1)} - \mathrm{e}^{-b(\beta-1)})(\tau + \rho\sin\theta)(\rho + \tau\sin\theta)/\beta^2,
\end{gathered}$$

TABLE 1

Coordinates (f, l) of the Boundary Points of the Main Stability Region for the Morse Potential for $b = 6$, Geometrical Parameters of the Cell θ, ρ, τ, α, and β, and Potential Energy V

f	l	θ	ρ	τ	α	β	V
−0.3605	0	0	0.802	0.548	0.972	0.972	0.095
−0.36	0.096	0.013	0.802	0.549	0.966	0.978	0.094
−0.35	0.376	0.053	0.809	0.549	0.953	1.001	0.081
−0.33	0.610	0.099	0.825	0.547	0.944	1.034	0.055
−0.30	0.780	0.181	0.870	0.545	0.939	1.107	0.018
−0.25	0.732	0.189	0.889	0.526	0.944	1.115	−0.021
−0.20	0.675	0.190	0.898	0.518	0.948	1.118	−0.061
−0.15	0.619	0.187	0.904	0.513	0.952	1.119	−0.100
−0.10	0.563	0.182	0.908	0.509	0.957	1.118	−0.140
−0.05	0.507	0.174	0.911	0.505	0.962	1.115	−0.181
0	0.452	0.169	0.916	0.502	0.968	1.116	−0.222
0.05	0.397	0.160	0.919	0.499	0.974	1.114	−0.263
0.10	0.343	0.155	0.925	0.497	0.980	1.115	−0.305
0.15	0.289	0.143	0.928	0.495	0.987	1.112	−0.347
0.20	0.235	0.128	0.930	0.493	0.996	1.107	−0.390
0.25	0.184	0.124	0.940	0.491	1.005	1.113	−0.434
0.30	0.132	0.104	0.943	0.490	1.017	1.107	−0.478
0.35	0.083	0.091	0.954	0.488	1.031	1.110	−0.523
0.40	0.035	0.059	0.963	0.487	1.053	1.104	−0.569
0.44	0	0	0.981	0.486	1.095	1.095	−0.607

$$V_{\theta\theta} = b(2\,\mathrm{e}^{-2b(\alpha-1)} - \mathrm{e}^{-b(\alpha-1)})(\rho\tau\cos\theta/\alpha)^2$$
$$-(\mathrm{e}^{-2b(\alpha-1)} - \mathrm{e}^{-b(\alpha-1)})\rho\tau(\alpha^2\sin\theta - \rho\tau\cos^2\theta)/\alpha^3$$
$$+ (\mathrm{e}^{-2b(\beta-1)} - \mathrm{e}^{-b(\beta-1)})\rho\tau(\beta^2\sin\theta + \rho\tau\cos^2\theta)/\beta^3$$
$$+ b(2\,\mathrm{e}^{-2b(\beta-1)} - \mathrm{e}^{-b(\beta-1)})(\rho\tau\cos\theta/\beta)^2 + l\tau\sin\theta,$$
$$V_{\theta\tau} = \rho\cos\theta[-b(2\,\mathrm{e}^{-2b(\alpha-1)} - \mathrm{e}^{-b(\alpha-1)})\tau(\tau - \rho\sin\theta)/\alpha^2$$
$$+ (\mathrm{e}^{-2b(\alpha-1)} - \mathrm{e}^{-b(\alpha-1)})\rho(\rho - \tau\sin\theta)/\alpha^3 - (\mathrm{e}^{-2b(\beta-1)} - \mathrm{e}^{-b(\beta-1)})\rho(\rho + \tau\sin\theta)/\beta^3$$
$$+ b(2\,\mathrm{e}^{-2b(\beta-1)} - \mathrm{e}^{-b(\beta-1)})\tau(\tau + \rho\sin\theta)/\beta^2] - l\cos\theta,$$
$$V_{\tau\tau} = b(2\,\mathrm{e}^{-2b(\alpha-1)} - \mathrm{e}^{-b(\alpha-1)})(\tau - \rho\sin\theta)^2/\alpha^2$$
$$- (\mathrm{e}^{-2b(\alpha-1)} - \mathrm{e}^{-b(\alpha-1)})\rho^2\cos^2\theta/\alpha^3 - (\mathrm{e}^{-2b(\beta-1)} - \mathrm{e}^{-b(\beta-1)})\rho^2\cos^2\theta/\beta^3$$
$$+ b(2\,\mathrm{e}^{-2b(\beta-1)} - \mathrm{e}^{-b(\beta-1)})(\tau + \rho\sin\theta)^2/\beta^2 + 2b(2\,\mathrm{e}^{-2b(2\tau-1)} - \mathrm{e}^{-b(2\tau-1)}).$$

In all these expressions, the positive factor $2bAg^{-6}$ is omitted, which has no effect on the signs of the principal minors of the Hessian matrix.

The approximate coordinates $(f,\ l)$ of some boundary points of the stability region of the unit cell with respect to the Morse potential function for $b = 6$ and the corresponding values of the geometrical parameters defining the cell configuration are listed in Table 1. (In Tables 1–5, the values of θ, ρ, and τ are given with three significant figures since two-figures accuracy in specifying these parameters as initial data is frequently insufficient for the convergence of the Newton method to the solution defining the stable configuration of the cell.) The last column contains values of the potential function calculated by formula (2) and normalized by $2bAg^{-6}$. In Table 2, the boundary values of l for which the second stable configuration of the unit cell is possible and its geometrical characteristics are given for the same value of $b = 6$ and some values of f. For example, for $f = -0.3$ and $l = 0.467$, in addition to the solution (θ, ρ, τ) given in Table 2, the following three solutions are possible: (0.072, 0.796, 0.58), (0.746, 1.234, 0.523), and (0.074, 0.831, 0.528); the last solution corresponds to stable equilibrium.

Calculation results for $b = 1$ are given in Table 3.

TABLE 2

Coordinates (f, l) of the Boundary Points of the Supplementary Stability Region in the Case of the Morse Potential for $b = 6$, Geometrical Parameters of the Cell θ, ρ, τ, α, and β, and Potential Energy V

f	l	θ	ρ	τ	α	β	V
−0.3605	0.563	1.435	1.478	0.527	0.958	2.001	0.123
	0.551	0.953	1.338	0.531	0.956	1.797	0.129
−0.36	0.563	1.543	1.485	0.527	0.959	2.011	0.123
	0.550	0.939	1.332	0.531	0.956	1.788	0.129
−0.35	0.546	1.429	1.476	0.525	0.959	1.998	0.117
	0.535	0.966	1.344	0.528	0.957	1.804	0.122
−0.30	0.467	1.509	1.481	0.519	0.964	1.999	0.084
	0.459	0.996	1.356	0.521	0.962	1.816	0.088
−0.25	0.388	1.431	1.475	0.514	0.968	1.986	0.050
	0.384	1.088	1.394	0.515	0.967	1.865	0.052
−0.20	0.310	1.364	1.468	0.511	0.973	1.970	0.016
	0.309	1.223	1.438	0.511	0.973	1.926	0.017
−0.15	0.233	1.251	1.447	0.508	0.979	1.936	−0.019

TABLE 3

Coordinates (f, l) of the Boundary Points of the Stability Region in the Case of the Morse Potential for $b = 1$, Geometrical Parameters of the Cell θ, ρ, τ, α, and β, and Potential Energy V

f	l	θ	ρ	τ	α	β	V
−0.179	0	0	0.615	0.644	0.890	0.890	−1.111
−0.15	0.196	0.204	0.666	0.632	0.820	1.006	−1.142
−0.10	0.360	0.372	0.751	0.628	0.785	1.141	−1.207
−0.05	0.528	0.574	0.895	0.632	0.766	1.347	−1.295
−0.03	0.642	0.995	1.213	0.597	0.782	1.744	−1.360
−0.02	0.621	1.027	1.229	0.582	0.791	1.753	−1.362
0	0.582	1.075	1.254	0.562	0.806	1.769	−1.367
0.05	0.491	1.052	1.256	0.530	0.838	1.736	−1.387
0.10	0.408	1.056	1.279	0.508	0.873	1.740	−1.413
0.15	0.329	0.976	1.276	0.492	0.911	1.705	−1.443
0.20	0.256	0.925	1.292	0.478	0.955	1.699	−1.478
0.25	0.187	0.799	1.286	0.467	1.006	1.653	−1.518
0.30	0.125	0.696	1.300	0.458	1.067	1.632	−1.563
0.35	0.070	0.558	1.317	0.450	1.144	1.601	−1.614
0.40	0.025	0.386	1.348	0.445	1.250	1.571	−1.671
0.446	0	0	1.399	0.441	1.467	1.467	−1.731

Stability Region for the Lennard-Jones Potential. In this case, the interaction potential of two atoms is given by [8]

$$v(\gamma) = Ag^{-6}(\gamma^{-12}/2 - \gamma^{-6}) \tag{10}$$

and system (3) for determining the equilibrium state of the cell for given values of f and l is written as

$$\begin{gathered}(1/\alpha^8 - 1/\alpha^{14})(\rho - \tau\sin\theta) + (1/\beta^8 - 1/\beta^{14})(\rho + \tau\sin\theta) - f = 0,\\ \rho(-1/\alpha^8 + 1/\alpha^{14} + 1/\beta^8 - 1/\beta^{14}) - l = 0,\\ 1/\alpha^8 - 1/\alpha^{14} + 1/\beta^8 - 1/\beta^{14} + 2/(2\tau)^8 - 2/(2\tau)^{14} = 0,\end{gathered} \tag{11}$$

where $f = Fg^7/(6A)$, $l = Lg^7/(6A)$, and the functions α and β and their derivatives are found from relations (1) and (5). The stability of the obtained equilibrium state is studied using the Sylvester criterion after substitution of the solution (ρ, θ, τ) of system (11) into the expressions for the second derivatives of the function (2) normalized by $12Ag^{-6}$:

$$V_{\rho\rho} = 13/\alpha^{14} - 7/\alpha^8 + 13/\beta^{14} - 7/\beta^8 - (14/\alpha^{16} - 8\alpha^{10} + 14/\beta^{16} - 8/\beta^{10})(\tau\cos\theta)^2,$$

TABLE 4

Coordinates (f, l) of the Boundary Points of the Stability Region in the Case of the Lennard-Jones Potential, Geometrical Parameters of the Cell θ, ρ, τ, α, and β, and Potential Energy V

f	l	θ	ρ	τ	α	β	V
−0.327	0	0	0.809	0.543	0.975	0.975	0.093
−0.30	0.585	0.097	0.832	0.545	0.949	1.038	0.056
−0.277	0.708	0.176	0.876	0.543	0.947	1.108	0.029
−0.25	0.681	0.183	0.890	0.529	0.949	1.114	0.012
−0.20	0.625	0.177	0.896	0.519	0.953	1.111	−0.023
−0.15	0.570	0.178	0.904	0.513	0.957	1.115	−0.061
−0.10	0.514	0.168	0.906	0.508	0.961	1.110	−0.099
−0.05	0.459	0.164	0.911	0.505	0.966	1.111	−0.139
0	0.404	0.156	0.914	0.502	0.971	1.109	−0.178
0.05	0.349	0.146	0.916	0.499	0.977	1.105	−0.219
0.10	0.295	0.137	0.920	0.497	0.984	1.103	−0.259
0.15	0.242	0.129	0.925	0.495	0.991	1.104	−0.301
0.20	0.189	0.116	0.929	0.493	1.000	1.101	−0.343
0.25	0.138	0.107	0.937	0.491	1.010	1.103	−0.386
0.30	0.087	0.086	0.943	0.490	1.024	1.099	−0.430
0.35	0.039	0.062	0.954	0.488	1.044	1.098	−0.475
0.399	0	0	0.982	0.487	1.096	1.096	−0.520

$$V_{\rho\theta} = \tau\cos\theta[(2/\alpha^{16} - 1/\alpha^{10} + 2/\beta^{16} - 1/\beta^{10})6\rho\tau\sin\theta$$

$$+ (1/\alpha^{16} - 1/\alpha^{10} - 1/\beta^{16} + 1/\beta^{10})\tau^2 - (13/\alpha^{16} - 7/\alpha^{10} - 13/\beta^{16} + 7/\beta^{10})\rho^2],$$

$$V_{\rho\tau} = (14/\alpha^{16} - 8/\alpha^{10} + 14/\beta^{16} - 8/\beta^{10})\rho\tau\cos^2\theta - (13/\alpha^{14} - 7/\alpha^{8} - 13/\beta^{14} + 7/\beta^{8})\sin\theta,$$

$$V_{\theta\theta} = (14/\alpha^{16} - 8/\alpha^{10} + 14/\beta^{16} - 8/\beta^{10})(\rho\tau\cos\theta)^2,$$

$$V_{\theta\tau} = -l\cos\theta + \rho\cos\theta[(2/\alpha^{16} - 1/\alpha^{10} + 2/\beta^{16} - 1/\beta^{10})6\rho\tau\sin\theta$$

$$+ (1/\alpha^{16} - 1/\alpha^{10} - 1/\beta^{16} + 1/\beta^{10})\rho^2 - (13/\alpha^{16} - 7/\alpha^{10} - 13/\beta^{16} + 7/\beta^{10})\tau^2],$$

$$V_{\tau\tau} = 13/\alpha^{14} - 7/\alpha^{8} + 13/\beta^{14} - 7/\beta^{8} + 2[13/(2\tau)^{14} - 7/(2\tau)^{8}]$$

$$- (14/\alpha^{16} - 8\alpha^{10} + 14/\beta^{16} - 8/\beta^{10})(\rho\cos\theta)^2.$$

Table 4 gives the approximate coordinates (f, l) of some boundary points of the stability region of the unit cell for the Lennard-Jones potential.

We now analyze in greater detail some particular cases of equilibrium states of the cell. For $\tau = 1/2$, the third equation of system (11) becomes

$$1/\alpha^8 - 1/\alpha^{14} + 1/\beta^8 - 1/\beta^{14} = 0. \tag{12}$$

If $\theta = 0$ (i.e., $\alpha = \beta$), the only equilibrium state is the initial configuration of the cell $\alpha = \beta = 1$ for $f = l = 0$. We consider the auxiliary function $t(x) = 1/x^8 - 1/x^{14}$ for $x > 0$, which increases monotonically to $t_{\max} \approx 0.203$ at the point $x_{\max} = (7/4)^{1/6} \approx 1.098$ and then decreases monotonically to zero; $t(x) < 0$ for $x < 1$ and $t(x) > 0$ for $x > 1$. In this case, if $\alpha \neq \beta$ (i.e., $\theta \neq 0$), then for each value of $\alpha < 1$, Eq. (12) admits two solutions $1 < \beta_1 < 1.098 < \beta_2$ that correspond to two possible equilibrium states, one of which is stable. We note that the first two equations of system (11) can be used to calculate the values of f and l for which precisely these equilibrium states occur: (α, β_1) and (α, β_2). In addition, from (12) it follows that for $\tau = 1/2$ and $\theta \neq 0$, equilibrium of the cell is impossible in the case where α and β are smaller or large than unity simultaneously.

For $\tau = 1/2$, the first equation of system (11) combined with (12) yields $f = (1/\beta^8 - 1/\beta^{14})\sin\theta$. It follows that f vanishes only for the initial configuration of four atoms, i.e., equilibrium of the cell is impossible for $f = 0$, $\tau = 1/2$, and $l \neq 0$ ("pure shear without compression").

TABLE 5

Coordinates (f, l) of the Boundary Points of the Stability Region in the Case of the Lennard-Jones Potential for $\tau = 1/2$ (Incompressible Vertical Chains of the Close-Packed Atomic Layer), Geometrical Parameters of the Cell θ, ρ, α, and β, and Potential Energy V

f	l	θ	ρ	τ	α	β	V
−0.5	0.974	0.214	0.902	0.5	0.934	1.120	0.223
−0.4	0.858	0.207	0.905	0.5	0.939	1.120	0.145
−0.3	0.742	0.192	0.904	0.5	0.946	1.113	0.066
−0.2	0.628	0.181	0.906	0.5	0.953	1.111	−0.014
−0.1	0.515	0.168	0.909	0.5	0.961	1.108	−0.095
0	0.404	0.155	0.913	0.5	0.971	1.107	−0.177
0.1	0.295	0.140	0.920	0.5	0.984	1.107	−0.261
0.2	0.188	0.117	0.927	0.5	1.000	1.103	−0.346
0.3	0.085	0.085	0.938	0.5	1.025	1.100	−0.434
0.397	0	0	0.977	0.5	1.097	1.097	−0.524

For $\theta = 0$ ($\alpha = \beta$), the third equation of system (11) becomes

$$-1/\alpha^8 + 1/\alpha^{14} = 1/(2\tau)^8 - 1/(2\tau)^{14}. \tag{13}$$

The solutions of this equation are values $1 < \alpha_1 < 1.098 < \alpha_2$ for $\tau < 1/2$ and values $\alpha < 1$ for $\tau > 1/2$. The maximum value of τ ($\tau > 1/2$) for which a solution of Eq. (13) and, hence, an equilibrium state exists is equal to $\tau = (7/4)^{1/6}/2 \approx 0.549$, which corresponds to the values given in the first row in Table 4. The minimum value of τ ($\tau < 1/2$) for which an equilibrium state exists is a root of the equation $-1/x^8 + 1/x^{14} - \varepsilon = 0$ or $x^2(1/x^8)^2 - 1/x^8 - \varepsilon = 0$, where $x = 2\tau$ and $\varepsilon = (4/7)^{4/3} - (4/7)^{7/3}$. It follows that $1/x^8 = (1 + \sqrt{1 + 4\varepsilon x^2})/(2x^2)$ $< (1 + \sqrt{1 + 4\varepsilon})/(2x^2)$ or $\tau > [2/(1 + \sqrt{1 + 4\varepsilon})]^{1/6}/2 \approx 0.487$, which corresponds to the values given in the last row in Table 4. In this case, from the first equation of system (11), we obtain the formula $f = 2\rho(1/\alpha^8 - 1/\alpha^{14})$ for the tensile load whose magnitude is slightly larger than the value calculated by formula (56) of [3] since $\alpha^2 < \rho^2 + 1/4$ by virtue of the fact that the value of $\tau \approx 0.487$ is slightly less than 1/2.

Finally, if $\tau \neq 1/2$ or $\theta \neq 0$, the third equation of system (11) admits an infinite number of solutions, some of which may correspond to stable equilibrium states of the unit cell.

Table 5 lists the results of similar calculations obtained for the additional condition $\tau = 1/2$, which is equivalent to the condition that the length of close-packed atomic chains remains unchanged under rotation, i.e., Poisson's ratio vanishes. In this case, the system of equilibrium equations contains only two equations $V_\rho = 0$ and $V_\theta = 0$. These equations are studied in detail in [3] for the tension-shear region ($f > 0$).

Discussion of the Results. Figure 2 shows the boundaries of the stability regions constructed from the data given in Tables 1–5 (curves 1–5, respectively). The boundaries are shown only in the upper half-plane since the stability region is symmetric about the f axis. Indeed, if a point with coordinates (f, l) corresponds to an equilibrium state of the cell, system (6)–(8) has a solution $(\rho, \tau, \theta, \alpha, \beta)$. One can readily verify that in this case the set of quantities $(\rho, \tau, -\theta, \beta, \alpha)$ is the solution of system (6)–(8) for the point $(f, -l)$. Consequently, the point $(f, -l)$ symmetric to the point (f, l) is also an equilibrium point of the unit cell. In a similar manner, the simultaneous stability of the symmetric equilibrium states (f, l) and $(f, -l)$ is analyzed analytically using the Hessian matrix. The calculation results confirm the validity of the conclusions, thereby supporting the adequacy of the mathematical model to physical considerations.

In Fig. 2, circles show the variation in the unit-cell configuration along the boundaries of the stability regions for various magnitudes and direction of the forces f and l. One can see that the boundaries of the stability regions for the cases $\tau \neq 1/2$ and $\tau = 1/2$ (curves 4 and 5, respectively) differ only slightly for $f = -0.25$–0.40. Similar curves (see [10, Figs. 4 and 5]) were obtained for the stressed state of a three-atomic cell. We note that curve 5 in Fig. 2 is a nearly straight line, which agrees with the results of [3] only for $f > 0$, i.e., for tension-shear loading.

For all the points (f, l) listed in Tables 1–5, we also calculated the "atomic volume" $S = 2\rho\tau\cos\theta$ as the area of a parallelogram whose vertices are located at the centers of the atoms of the unit cell. We note that $S = \sqrt{3}/2 \approx 0.866$ for the unloaded initial cell. The maximum value of the volume is attained for $l = 0$ and $f > 0$, i.e., for the maximum tensile load, and it is equal to $S \leqslant 0.977$ for the points given in Tables 1, 4, and 5 and $S = 1.234$ for the points given in Table 3. The minimum value is $S \geqslant 0.866$ for the points given in Tables 1, 4, and 5

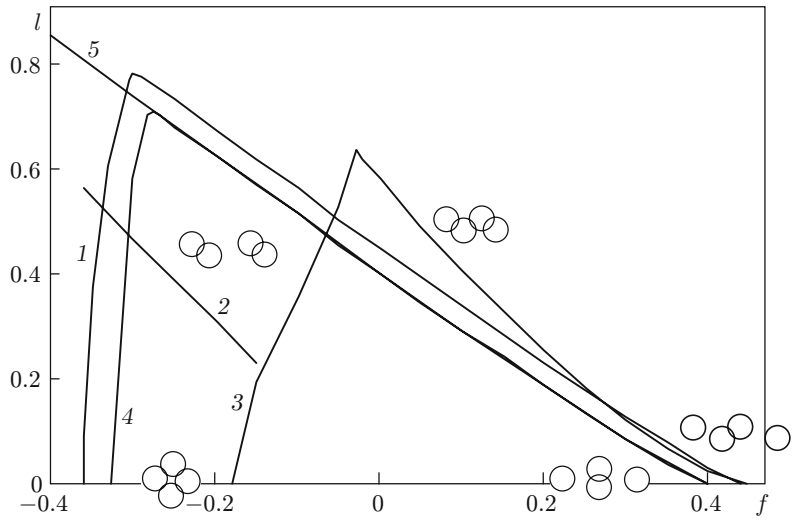

Fig. 2. Stability-region boundaries constructed for the data given in Tables 1–5 (curves 1–5, respectively).

and $S = 0.66$ for the points given in Table 3. Moreover, for the points listed in Tables 1, 3, 4, and 5, the area S reaches the local maximum $S \leqslant 0.950$ for the maximum value of l. For all points given in Table 2, the value of S varies from 0.044 to 0.835. These casts some doubt on the physical possibility of the second stable configuration.

If the interatomic distances are equal approximately to the atomic diameters, the Lennard-Jones potential (10) is almost identical to the Morse potential (4) for $b = 6$. Indeed, setting $\alpha = 1 + x$ and $x \approx 0$, we expand the potentials in the Maclaurin series:

$$\mathrm{e}^{-2b(\alpha-1)}/2 - \mathrm{e}^{-b(\alpha-1)} = \mathrm{e}^{-2bx}/2 - \mathrm{e}^{-bx} = -1/2 + (bx)^2/2 - (bx)^3/2 + \ldots$$

$$= -1/2 + (6x)^2/2 - (6x)^3/2 + \ldots \approx -1/2 + 36x^2/2 - 252x^3/2 + \ldots$$

$$= (1+x)^{-12}/2 - (1+x)^{-6} = \alpha^{-12}/2 - \alpha^{-6}.$$

One might expect that the behavior of the unit cell described by the Morse potential for $b = 6$ would be in agreement with that described by the Lennard-Jones potential since $2\tau \approx 1$, $\alpha \approx 1$, and $\beta \approx 1$ (see Table 1). This assumption is supported by calculation results (see Tables 1 and 4 and curves 1 and 4 in Fig. 2).

Figure 3 shows the boundaries of the stability regions of the unit cell for the ranges $0.20 \leqslant f \leqslant 0.45$ and $-0.24 \leqslant l \leqslant 0.24$ in the case of the Morse potential for $b = 6$ (curve 1) and $b = 1$ (curve 3). The behavior of curves 1 and 3 in this range corresponds to the Coulomb–Mohr fracture criterion considered in [11], where truncation of the fracture surface in the tension-compression region is discussed. Coulomb assumed that the failure process is affected by "internal friction." Mohr proposed the hypothesis that failure begins at the moment when the shear stress at an arbitrary site reaches a limiting value that is a function of the normal stress at this site. Therefore, the fracture criterion corresponding to the equation of the straight-line envelope of all large Mohr's circles, which, in turn, correspond to the onset of failure, is called the Coulomb–Mohr criterion. Previously, it has been shown [11] that the limiting curve represented by a linear envelope gives a fracture criterion suitable for many brittle materials. In the case considered, the calculation results show that the Coulomb–Mohr approximation is acceptable if the force f varies from -0.25 to 0.40 (curve 1 for the Morse potential for $b = 6$ and curve 4 corresponding to the Lennard-Jones potential in Fig. 2). One might expect that the critical loads obtained in a macroexperiment for a close-packed layer would be close to those corresponding to points of the limiting curves.

We note that for the compression-shear loading, the behavior of the boundaries of the stability region obtained numerically is in good agreement with the theoretical predictions of [12].

Conclusions. The stability region of a four-atom rhombic unit cell corresponding to a close-packed atomic layer was obtained numerically using the Morse and Lennard-Jones potentials for two parameters modeling tension and compression along the major diagonal of the cell and shear. The continuous closed first branch of the curve of

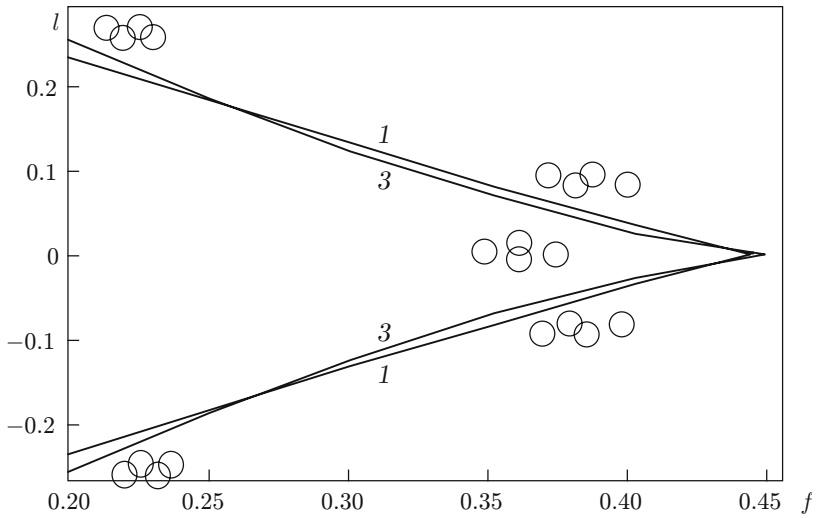

Fig. 3. Pointed part of the stability-region boundary for the Morse potential: curve 1 refers to $b = 6$ and curve 3 to $b = 1$.

the critical stable states (curves 1, 3, and 4 in Fig. 2) was constructed for the entire loading range considered. It was found that for a four-atom cell, the Lennard-Jones potential is almost equivalent to the particular case of the Morse potential for $b = 6$. A subregion of the stability region was found in which two different stable configurations of the cell exist for the same loading conditions. For some parts of the boundaries of the stability region, the calculation results were compared and found to be consistent with the data available in the literature. It was shown that for tension–shear loading, Poisson's effect can be ignored but for compression–shear loading, the boundary of the stability region has a different shape.

The loading conditions used in the numerical calculations for the four-atom cell correspond to the complex loading of Plexiglas specimens in [13]. The experiments of [13] showed that the critical loads are nearly equal for simple (proportional) and complex loads (see [13]). Thus, the macroscopic mechanical properties of a solid can be inferred from the limiting curves obtained for close-packed atomic layers.

It is likely that the pointed part of the stability-region boundary (see curves 1 and 3 in Fig. 3) has not been found experimentally since "pure tension without shear" is difficult to simulate because of the effect of the fixing conditions, which was discussed in [13–15]. A large scatter of experimental values of the critical loads is expected in the neighborhood of this pointed part.

This work was supported by the Russian Foundation for Basic Research (Grant No. 04-01-00191) and RAS Integration Project No. 4.11.3.

REFERENCES

1. G. P. Cherepanov, *Mechanics of Brittle Fracture*, McGraw-Hill, New York (1979).
2. F. A. McClintock and G. R. Irwin, "Plasticity aspects of fracture mechanics," in: *Fracture Toughness Testing and its Application Fracture Touchness Testing and Its Applications*, ASTM STP (1965).
3. J. M. T. Thompson, *Instabilities and Catastrophies in Science and Engineering*, Wiley, Chichester (1982).
4. N. H. Macmillan and A. Kelly, "The mechanical properties of perfect crystals," *Proc. Roy. Soc. London, Ser. A.*, **330**, 291–308 (1972).
5. R. M. J. Cotterill and M. Doyama, "Energy and atomic configurations of complete and dissociated dislocations. I. Edge dislocation in an fcc metal," *Phys. Rev.*, **145**, No. 2, 465-478 (1966).
6. J. W. Christian, *The Transformations in Metals and Alloys*, Part I: *Thermodynamics and General Kinetic Theory*, Pergamon Press, Oxford (1975).
7. M. W. Finnis and J. E. Sinclair, "A simple empirical N-body potential for transition metals," *Philos. Mag., Ser. A*, **50**, No. 1, 45–55 (1984).

8. J. M. T. Thompson and P. A. Shorrock, "Bifurcational instability of an atomic lattice," *J. Mech. Phys. Solids*, **23**, 21–37 (1975).
9. N. S. Astapov and V. M. Kornev, "Shear strain effects on the theoretical strength of an atomic lattice," *J. Appl. Mech. Tech. Phys.*, **40**, No. 4, 739–743 (1999).
10. V. M. Kornev and V. D. Kurguzov, "A discrete-integral strength criterion for complicated stress states," *Fatigue Fract. Eng. Mat. Struct.*, **22**, 989–995 (1999).
11. B. Paul, "Macroscopic criteria for plastic flow and brittle fracture," in: H. Liebowitz (ed.), *Fracture*, Vol. 2, Academic Press (1968).
12. J. Handin, "Strength and ductility," in: S. P. Clark, Jr. (ed.), *Handbook of Physical Constants* (1966), pp. 223–300.
13. L. V. Baev and S. N. Korobeinikov, "Buckling of a circular cylindrical Plexiglas shell under torsion and axial loading," *Mekh. Polimer.*, No. 6, 1051–1057 (1977).
14. V. M. Kornev and Yu. V. Tikhomirov, "Deformation and stability loss of a part of the atomic chain at the tip of a crack," *J. Appl. Mech. Tech. Phys.*, **34**, No. 3, pp. 439–448 (1993).
15. N. H. Macmillan "The ideal strength of solids," in: *Atomistics of Fracture*, R. Latanision and J. R. Pickens (eds.), Plenum Press, New York (1983), pp. 95–164.